Article

Black PEO Coatings on Titanium and Titanium Alloys Produced at Low Current Densities

Lorena Kostelac [1], Luca Pezzato [1,*], Elena Colusso [1], Marta Maria Natile [2], Katya Brunelli [1] and Manuele Dabalà [1]

[1] Department of Industrial Engineering, University of Padova, Via F. Marzolo 9, 35131 Padova, Italy; lorena.kostelac@phd.unipd.it (L.K.); elena.colusso@unipd.it (E.C.); katya.brunelli@unipd.it (K.B.); manuele.dabala@unipd.it (M.D.)

[2] Institute of Condensed Matter Chemistry and Technologies for Energy (ICMATE), National Research Council (CNR) and Department of Chemical Sciences, University of Padova, Via F. Marzolo, 1, 35131 Padova, Italy; martamaria.natile@unipd.it

[*] Correspondence: luca.pezzato@unipd.it

Abstract: Black coatings were successfully formed on Grade 2 (G2) and Grade 5 (G5) titanium alloy by means of a direct-current Plasma Electrolytic Oxidation (PEO) process at a very low current density of 0.05 A/cm^2. The impact of two different treatment times (30 min and 60 min) was examined. The electrolyte for the PEO process was a phosphate base solution $Na_5P_3O_{10}$ containing $FeSO_4$ and $(NH_4)_6Mo_7O_{24}$ as coloring additives. PEO-coated samples were subjected to optical, morphological, structural, chemical, and electrochemical characterization. XRD, EDS, and XPS data analyses revealed that anion MoO_4^{2-} and metal cation Fe^{3+} were successfully incorporated into the coatings. The results demonstrated that PEO-coated samples prepared after 60 min exhibit a stronger black color than those created after 30 min, with an absorptance maximum of 0.86. Furthermore, all prepared PEO coatings improve the corrosion resistance of bare titanium. Among them, the 60-minute PEO coatings on both alloys were the ones with the best corrosion properties.

Keywords: Plasma Electrolytic Oxidation (PEO); black coatings; titanium alloys

1. Introduction

Titanium and its alloys are often employed in many fields, including biomedical, chemical, marine, aeronautics, astronautics, and automotive, due to their low weight, high specific strength, low elastic modulus, biocompatibility, low density, and corrosion resistance [1–6]. A wide range of titanium-based compounds are also used in decorative coatings. Their primary purpose is to enhance the visual appeal of consumer products [7]. In aeronautics and astronautics, titanium improves equipment stealth and extinction properties [5].

Ceramic coating stands out as a prominent surface coating method, and its importance continues to increase alongside current technological advancements [8]. Ensuring temperature balance in a spacecraft is essential. An effective method to do that is using thermal control coatings (ceramics). These coatings have significant implications for the spacecraft's successful operation in the extreme temperature conditions of space. They are applied to the surfaces of structural materials and are intended to have strong absorption and emission properties, frequently appearing as black coatings [9]. Black coatings are highly desirable in spacecraft internal components, notably electronic housing packages used for thermal regulation [10–14]. Furthermore, they are widely used in various surface treatments, serving functional and aesthetic purposes. They are commonly applied for decorative purposes on items such as optical devices, heating elements, instrument panels, and sports equipment and are even found in numerous industrial sectors such as 3C (Computers, Communications, and Consumer Electronics) [15] and adiabatic engines [16]. It is

worth noting that while we refer to these coatings as "black", no material can absorb 100% of light at all angles and wavelengths. Even objects that appear black reflect some light, making ideal black material impossible to obtain [17].

Plasma electrolytic oxidation (PEO), sometimes referred to as micro-arc oxidation [18], has evolved from traditional anodic oxidation methods [19,20]. It is a surface modification technique that can be applied to various materials, including aluminum, magnesium, titanium, and other valve metal alloys [14,18–21]. In contrast to traditional anodizing, PEO offers an environmentally friendly approach [5,22–24] that typically employs fewer toxic electrolytes, a method with lower preparation costs, and simplified processing steps [25,26].

Furthermore, PEO provides distinct advantages, such as the ability to produce thicker coatings while maintaining excellent corrosion resistance, as well as favorable tribological and thermal properties [24,27,28]. The increased voltage applied during PEO generates the dielectric breakdown of oxide films, resulting in the formation of plasma discharges on the surface of the treated sample [11]. Coatings are formed due to metal substrate oxidation, electrolysis, electrophoresis processes, and plasma thermochemical reactions. Different compounds, mainly oxides formed by electrolyte components, can be found in the obtained coatings [29]. The microstructure of the PEO coating is usually multi-layer and porous structures [30]. Several parameters can influence the microstructure of PEO coatings, such as the electric regime, the electrolyte composition, the process's length, and the substrate's chemical composition [10,27,31]. Among these factors, the electrolyte stands out as the most significant variable influencing coating properties, particularly the colors of the ceramic layers [18,32]. Furthermore, PEO coatings' multi-layered and porous structure can increase the specific surface area. This improvement helps incorporate desired elements into coatings and develop diverse functional coatings [30–33].

The critical elements of electrolytes used for the development of PEO black optical coatings fall into two broad groups: anions like VO^{3-}, WO_4^{2-}, MoO_4^{2-}, and transition metal cations, including Fe^{2+}, Cu^{2+}, Co^{2+}, Ni^{2+} and Zr^{4+} [19,26,34].

To the best of our knowledge, only two papers have discussed the preparation of black PEO coatings on Grade 2 (G2) titanium. These articles, authored by Guo et al. [5] and Han et al. [14], both employed a silica-based electrolyte. The former utilizes $[Cu(NH_3)_4]^{2+}$ as a coloring additive, while the latter, in contrast, did not employ any additives and concentrated on achieving the black color in the coating, which naturally arises from black titanium oxide.

Few research groups have contributed to the study of black coatings on Grade 5 (G5) titanium alloy. Tang et al. investigated the effects of various additives in phosphate-based electrolytes for the development of black coatings. Their study consists of several works that provide a comparative analysis of additives ($FeSO_4$, $Co(CH_3COO)_2$, $Ni(CH_3COO)_2$ and K_2ZrF_6) [33], the effect of different concentrations of $FeSO_4$ [35] and $Co(CH_3COO)_2$ [36] on coating formation. Another research group, led by Madhuri et al. [37,38], provided findings on the generation of gray-black coatings using only silicate and phosphate-based electrolytes and no additives. A third group of researchers has also published several papers on black coatings on the same alloy. Yao et al. investigated the effects of various additives ($FeSO_4$, $Co(CH_3COO)_2$, $Ni(CH_3COO)_2$ and $NaWO_4$) in phosphate-based electrolytes [39], the results of coating preparation without additives using a combination of silicate and phosphate-based electrolytes [40], and the influence of zirconium in two of their papers [41,42]. A more recent study of G5 titanium alloy can be found in the literature, authored by Yao et al. [9]. This research focuses on the development of black coatings using a complex base electrolyte together with various additives ($FeSO_4$, $Co(CH_3COO)_2$, NH_4VO_3). It is important to note that all the aforementioned studies employ pulse mode PEO treatment, frequently with high current density or voltage.

The absence of studies involving the direct-current mode of PEO treatment motivated our research. Our second goal was to prepare coatings at a deficient current regime and to try the application of a novel combination of additives, $FeSO_4$ and $(NH_4)_6Mo_7O_{24}$, for making black coatings on titanium and its alloy. Additionally, we chose G5 titanium

alloy as a substrate, which has a substantial number of reported works on the successful preparation of black PEO coatings on its surface. On the other hand, the lack of research on G2 titanium (commercially "pure" titanium) prompted us to use this alloy and compare it to the previously researched G5 alloy. Furthermore, this work investigated the differences between two PEO process times, 30 min and 60 min. The prepared coatings' morphology, chemical and phase composition, black intensity with UV-VIS spectroscopy, and electrochemical corrosion properties were also characterized.

2. Materials and Methods

In the present research, Grade 2 (G2) and Grade 5 (G5) titanium alloys were employed as substrates for the Plasma Electrolytic Oxidation (PEO) process. G2 alloy is known as commercially "pure" titanium [43] (nominal composition: Ti $\geq$ 90%, Fe $\leq$ 0.30%, O $\leq$ 0.25%, C $\leq$ 0.08%, N $\leq$ 0.03%, H $\leq$ 0.015%, purchased from Acciaierie Valbruna, Vicenza, Italy). G5 possesses a nominal composition of: Ti = 87.6–91%, Al = 5.5–6.75%, V = 3.5–4.5%, Fe $\leq$ 0.40%, O $\leq$ 0.2%, C $\leq$ 0.08%, N $\leq$ 0.05%, H $\leq$ 0.015%, and has been purchased from Acciaierie Valbruna, Vicenza Italy. Before treatment, the samples went through the standard metallography preparation. This included polishing with abrasive papers of varying grits (320, 500, 800, 1200, and 4000) and polishing with colloidal silica cloths (from Cloeren Technologies, Padova, Italy). Subsequently, they were cleaned with distilled water and degreased using C_2H_6O (Ethanol; Carlo Erba Reagents, Milan, Italy) via ultrasonic treatment for 5 min. The electrolyte used in the process consisted of a phosphate-based solution containing $Na_5P_3O_{10}$ (Sodium tripolyphosphate; Thermo Scientific, Milan, Italy), and two additives, $(NH_4)_6Mo_7O_{24}$ (Amonium heptamolybdate tetrahydrate; VWR Chemicals, Milan, Italy) and $FeSO_4$ (Iron (II) sulfate heptahydrate; Honeywell, Milan, Italy), to achieve a black color. A thermostatic bath was used to keep the solution at room temperature. A TDK-Lambda DC power supply with a capacity of 400 V/8 A, a carbon steel mesh, and a cooling system were used in the PEO process. The titanium substrate served as the anode during the process, while the carbon steel mesh was the cathode. Treatments were performed in galvanostatic mode, with low current density and long treatment durations. Table 1 contains detailed parameter information. Following the PEO treatment, the samples were rinsed with deionized water and dried with compressed air.

Table 1. PEO process parameters (Current Density, PEO Treatment Time, Additives) for preparing the black coatings on titanium alloys, G2 and G5.

Sample	Current Density A/cm^2	PEO Treatment Time min	$Na_5P_3O_{10}$ g/L	$(NH_4)_6Mo_7O_{24}$ g/L	$FeSO_4$ g/L
G2-30	0.05	30	108	10	4
G2-60	0.05	60	108	10	4
G5-30	0.05	30	108	10	4
G5-60	0.05	60	108	10	4

Optical reflectance measurements were performed with a Jasco V770 UV-VIS-NIR spectrophotometer equipped with an integrating sphere in the 300–2000 nm range. Solar absorptance (α) was calculated from reflectance spectra in the wavelength range 300–2000 nm according to the following equation:

$$\alpha = \frac{\int_{300\,\text{nm}}^{2000\,\text{nm}} I_{sol}(\lambda)(1 - R(\lambda))d\lambda}{\int_{300\,\text{nm}}^{2000\,\text{nm}} I_{sol}(\lambda)d\lambda} \tag{1}$$

Here, $R(\lambda)$ represents the spectral reflectance of the sample at a given wavelength λ, while $I_{sol}(\lambda)$ refers to the incident spectrum [34,44].

A Cambridge Stereoscan 440 Scanning Electron Microscope (SEM) (Leica Microsystem S.r.l., Milan, Italy) equipped with a Philips PV9800 Energy Dispersive Spectroscopy (EDS) system (Leica Microsystem S.r.l., Milan, Italy) was used to examine the morphological

characteristics of the PEO black coatings as well as the elemental composition of both the surface and cross-section of the samples. Samples were carefully cut, embedded in epoxy resin, and polished using traditional metallographic techniques before performing a cross-sectional analysis.

A stereo microscope Zeiss Stemi C-500 (Carl Zeiss, Jena, Germany) was used to obtain surface images of black PEO-coated samples to visualize the surface in its natural form. All image analysis was performed using the ImageJ software package (Version 1.53t 24 August 2022) [45].

Siemens D500 X-ray diffractometer (Siemens, Munich, Germany) using Cu Kα radiation with 2θ ranging from 10° to 90° (0.05° step size and 5 s counting time per step) working at 40 kV and 30 mA with Bragg–Brentano Geometry was used to characterize phases of samples surfaces.

X-ray Photoelectron Spectra (XPS) were measured with a ThermoFisher Escalab QXi spectrometer using a monochromatic Al Kα radiation and argon-assisted charge compensation. All signal positions are given in binding energy (BE). Both extended (survey: pass energy 100 eV; dwell time 20 ms; step 1 eV) and detailed spectra (for Ti 2p, Mo 3d, Fe 2p, P 2p, Na 1s, O 1s, C 1s with pass energy 25 eV; dwell time 50 ms; step 0.1 eV) were collected. Spectra were analyzed with ThermoFisher Advantage software (2023 version) using Shirley-type backgrounds and Gaussian–Lorentzian product line shapes. All quantifications were done from detailed spectra.

The corrosion characteristics of samples immersed in a 3.5% sodium chloride solution were evaluated using a Potentiodynamic Polarization test (PDP) and Electrochemical Impedance Spectroscopy (EIS). These electrochemical measurements were carried out at room temperature using a three-electrode corrosion cell and a GAMRY Interface 1010E potentiostat. The exposed surface area of the working electrodes of both PEO-coated and uncoated Ti alloys was 1.0 cm^2. The counter electrode was platinum, and the reference electrode was represented as Saturated Calomel Electrode (SCE). All recorded potentials in this study were referenced to the SCE scale. The frequency range of the EIS measurements was 10^{-2} Hz to 10^5 Hz, with 10 frequency points per logarithmic decade and a perturbation amplitude of 10 mV. The experimental data were subsequently fitted by two equivalent circuits using Gamry Echem Analyst software (number 7.9.0.11572). The PDP test was performed with a scan rate of 2 mV/s. Both the EIS and PDP measurements were performed in triplicate to ensure reproducibility.

3. Results

3.1. Optical Measurements

To determine the color and the darkness of the coatings, optical measurements were carried out with a stereo microscope observation and UV-VIS reflectance measurements. Stereo microscope images presented in Figure 1 can convey the appearance and the color of the coating's surface. It can be seen from the images that all treated samples, both on the G2 and G5 titanium alloys, are characterized by a dark, almost black color. However, by increasing the PEO treatment time from 30 min to 60 min, a black color with fewer brown spots characterizes the coatings.

The absorptance of the PEO-coated samples is reported in Table 2, and the reflectance spectra are shown in Figure 2. Absorptance (α) was determined from the reflectance spectra of the coatings, according to Equation (1) (see Methods). The lower the reflectance is, the better the absorptance is [34]. Based on the spectra in Figure 2, all prepared coatings reflect almost 10% of light in the visible range, with a maximum reflectance in the NIR range of about 35%. The calculated absorptance of the coatings is over 0.8 for all the tested conditions (see Table 2). As was visible from the stereo microscopic images, a blacker color is present in the coatings prepared with a prolonged processing time after 60 min of the PEO process, corresponding to an absorptance of 0.86, which is comparable to the results in the literature, where the reported solar absorptance of the PEO black coatings is in the range of 0.75 to 0.90 [13].
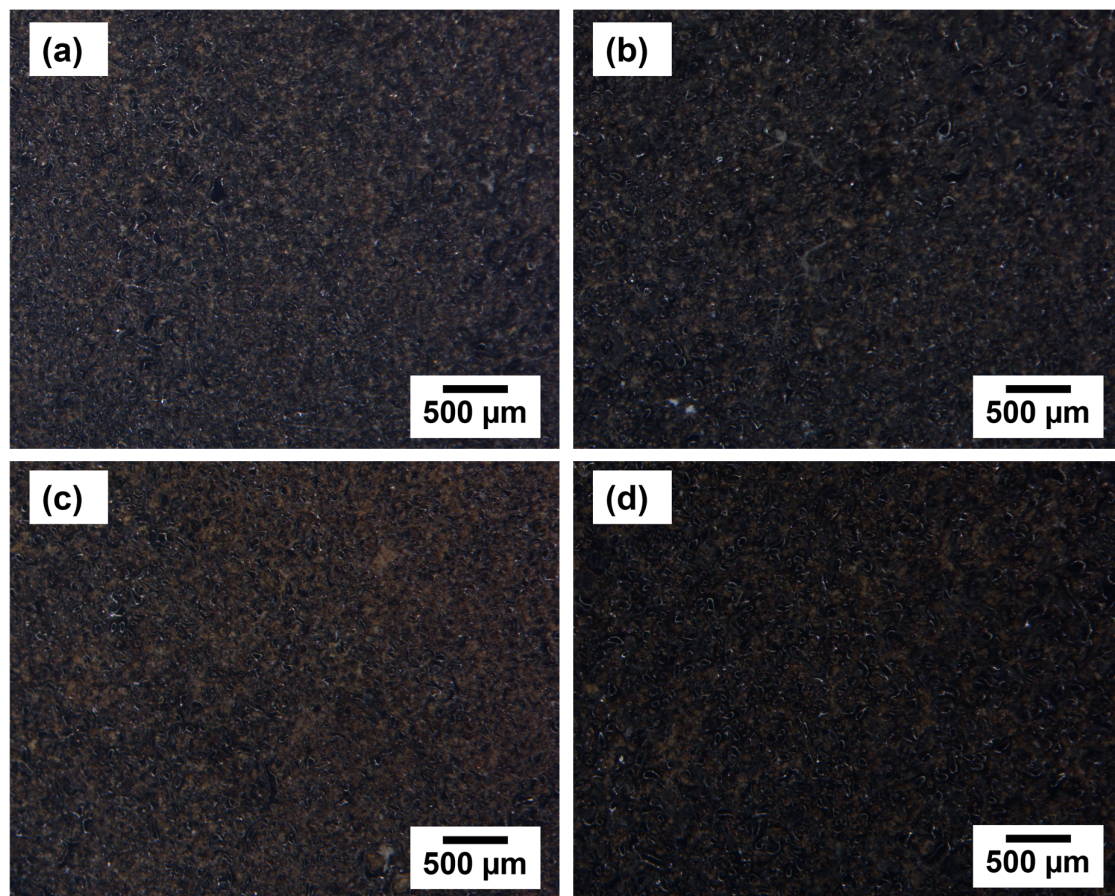
Figure 1. Stereo microscope images of PEO-coated samples on two different titanium alloys and with two different PEO treatment times: (**a**) G2-30, (**b**) G2-60, (**c**) G5-30, and (**d**) G5-60.

Table 2. The absorptance value of the PEO-coated samples.

Sample	Absorptance (α)
G2-30	0.84
G2-60	0.86
G5-30	0.84
G5-60	0.86

3.2. Morphology and Composition of the Black PEO Coatings

Surface SEM micrographs are reported in Figure 3. In general, the characteristic porous structure of PEO coatings can be seen in accordance with the literature [46,47]. Pores have a diameter of a few nanometers to micrometers in size. In fact, with the prolonged PEO process time, from 30 min to 60 min, a significant change in the morphology of the sample's surface is noticeable. PEO coatings obtained after 30 min have more pores of a smaller diameter, while with an increase in the processing time, there is also an increase in pores dimensions from nanometer to micrometer sizes, creating a channel structure. Yao et al. [9] reported similar results, where after extending the reaction time, the nano-pores were stacked and connected to form the micro-pores and particular channel structure.
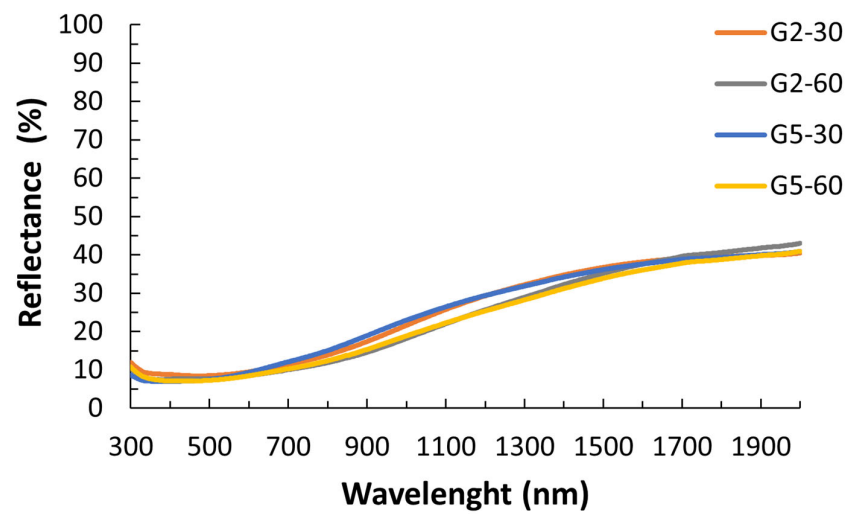
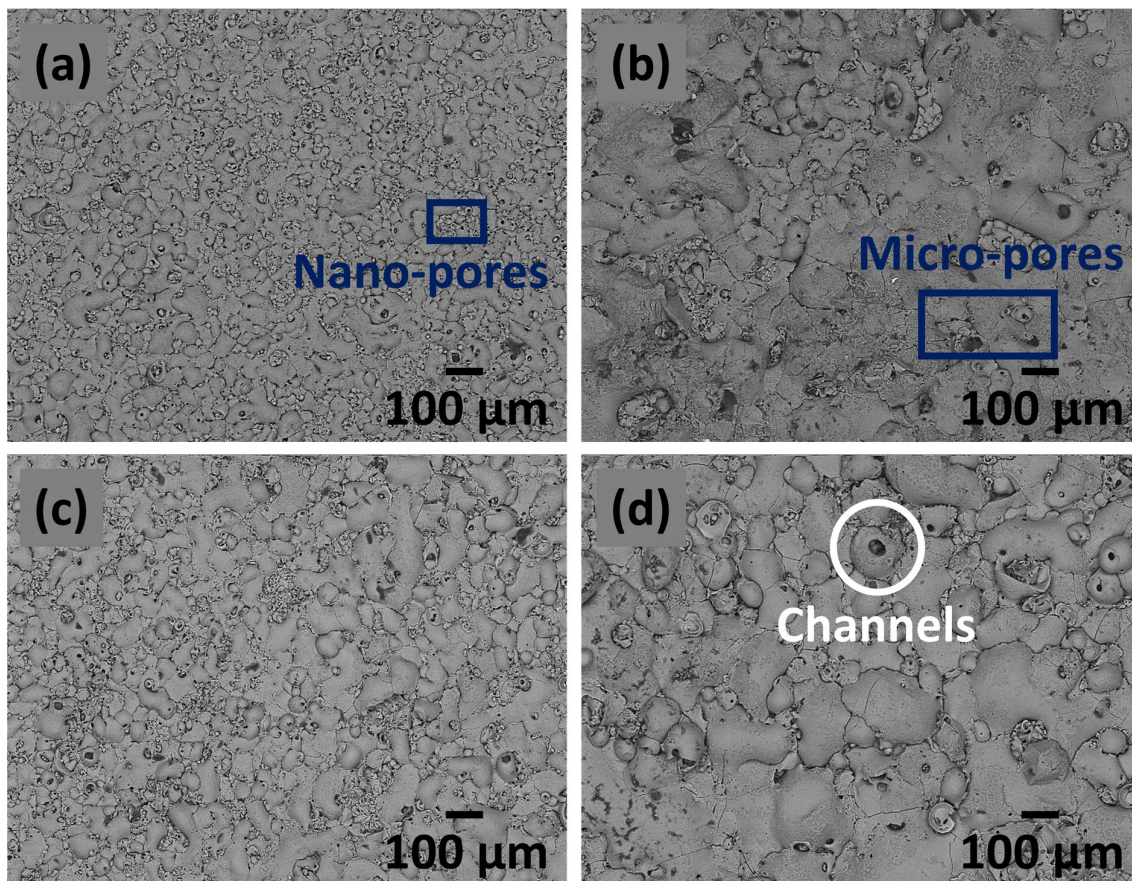**Figure 2.** Reflectance spectra of PEO-coated samples.

Figure 3. Surface SEM micrographs of black PEO coatings of the sample: (**a**) G2-30, (**b**) G2-60, (**c**) G5-30, and (**d**) G5-60.

Cross-section SEM micrographs are presented in Figure 4. In the micrographs, the titanium substrate is shown in gray, the epoxy resin in black, and there is a PEO coating between them. From the resulting images, the change in the compactness of the outer layer can be noticed by increasing the processing time. Likewise, after 30 min of the PEO processes, coatings contain many pores full of grooves and empty space. Although there is no significant change in the general thickness between the PEO coatings, a difference in

the barrier layer can be observed. The 30-minute coatings have an almost invisible inner barrier layer, while with the 60-minute coatings, it can be seen that this space is almost completely filled (indicated by arrows), suggesting a thicker inner barrier layer.
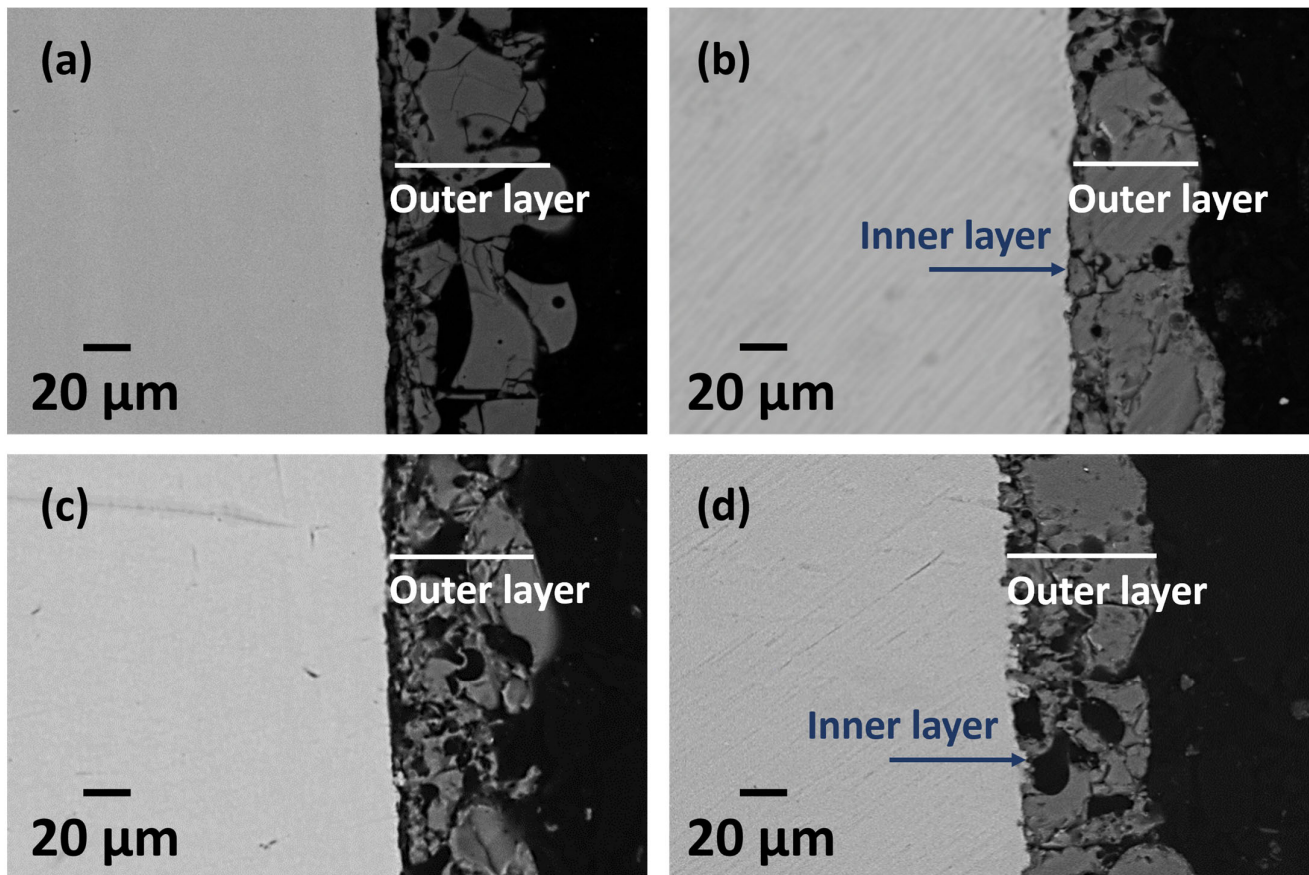
Figure 4. Cross-section SEM micrographs of black PEO coatings of the sample: (**a**) G2-30, (**b**) G2-60, (**c**) G5-30, and (**d**) G5-60.

Based on the EDS analysis of the surface and the cross-section, coatings consist of the following elements: O, Na, P, Mo, Ti, Fe, V, and Al, as shown in Table 3. In particular, coatings are rich in oxygen and phosphorus, with less iron, molybdenum, and sodium. The presence of molybdenum, iron, phosphorus, and sodium is due to the electrolyte used to prepare PEO coatings, while titanium, vanadium, and aluminum are from the substrate. Small amounts of vanadium and aluminum are present only in G5 titanium alloy, which is expected considering the chemical composition of titanium G5 [48]. Sodium is present only in the EDS analysis of the sample's surface, which may suggest that sodium compounds do not go in-depth in the coating.

3.3. XRD and XPS Characterization of the Black Coatings

XRD analysis was performed to evaluate the phase composition of coatings. Results are reported in Figure 5. The XRD was conducted on all treated samples, G2-30, G2-60, G5-30, and G5-60. All the pattern peaks are duly assigned using the 5.2.0 HighScore (Plus) software database. Similar results were obtained in all samples with a difference in the intensity of diffraction patterns. According to the database, the reflections of TiO_2 (anatase and rutile), Ti, Na_3PO_4, Na_2MoO_4, γFe_2O_3 can be distinguished. The reflections of crystalline Ti are due to the substrate, while all the other compounds can be found in PEO coatings. Two different mineral forms of TiO_2, anatase, and rutile, are typical for PEO coatings on titanium alloy substrates [49]. Diffraction peaks assigned to them are situated

at 2θ = 24.9°, 27.9°, 36.4°, 37.1°, 41.1°, 47.3°, 61.7°, respectively [ICSD 98-007-4532; ICSD 98-016-1908]. Na_3PO_4 (2θ = 20.9°, 22.5°, 33.1°, 46.0°, 47.5°) [ICSD 98-003-3719], Na_2MoO_4 (2θ = 21.0°, 23.8°, 29.6°, 30.3°, 47.1°) [ICSD 98-015-1972], γFe_2O_3 (2θ = 30.2°, 35.6°, 62.9°, 74.8°) [ICSD 98-017-2906] are all present in the PEO coating due to the composition of the used electrolyte. These XRD analyses are in accordance with the EDS and XPS data.

Table 3. Results of the Semi-quantitative EDS analysis of PEO-coated samples performed on the surface and the cross-section of samples. Results are present in Wt.%.

| Sample	Elements (Wt.%)							
	O	**Na**	**P**	**Mo**	**Ti**	**Fe**	**V**	**Al**
G2-30 surface	52.8	2.8	17.3	3.1	22.8	1.2	-	-
G2-30 cross-section	40.2	-	17.6	4.3	36.0	1.9	-	-
G2-60 surface	51.0	3.5	17.0	2.9	24.3	1.3	-	-
G2-60 cross-section	47.0	-	17.5	3.1	31.2	1.2	-	-
G5-30 surface	50.4	4.0	18.1	3.2	20.3	1.1	0.9	2.0
G5-30 cross-section	55.5	-	19.7	4.4	19.0	1.4	-	-
G5-60 surface	49.1	3.4	17.9	3.0	22.5	1.2	0.9	2.0
G5-60 cross-section	47.6	-	14.1	4.2	32.8	1.3	-	-
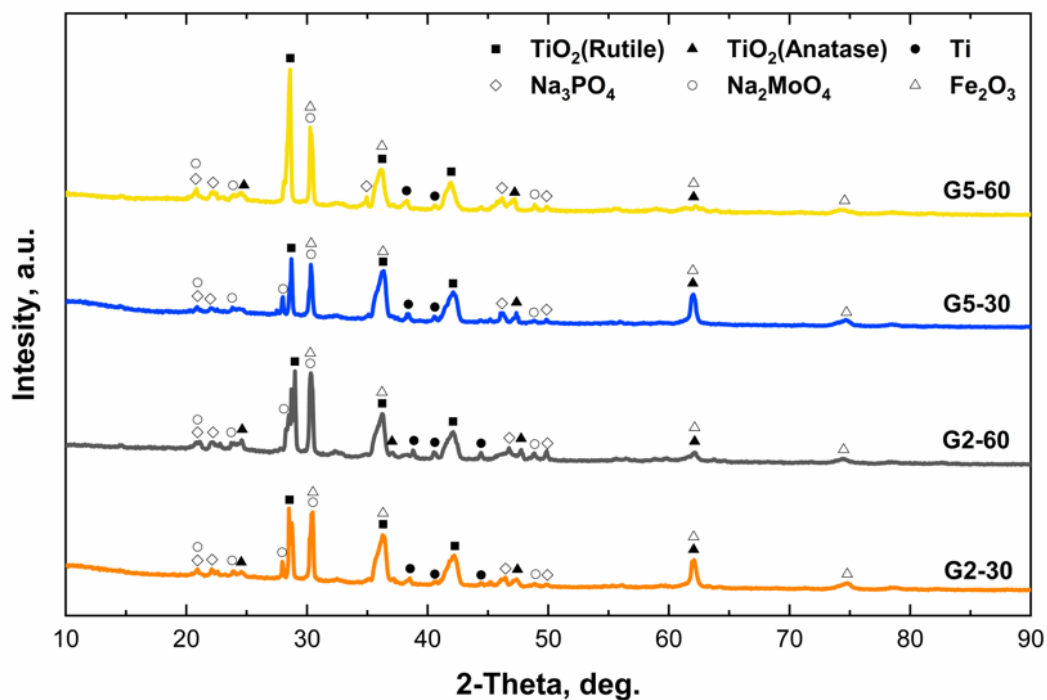
Figure 5. XRD patterns of PEO-coated samples: G2-30, G2-60, G5-30, and G5-60.

XPS analysis was carried out to investigate the kind and chemical state of elements on the samples' surface. The survey spectra of all PEO coatings on G2 and G5 titanium alloys reveal the presence on the surface of all the expected species, namely Ti, Mo, Fe, P, Na, O, and C. V contained in the G5 titanium alloy was not detected because of the small amount or not segregate on the surface. Traces of Al, N, and S derived from substrate and electrolytes were also observed.

The peak fitting analysis of the more relevant elements is reported in Figure 6. The peak shape and binding energies at 458.4 and 464.2 eV, respectively, for Ti $2p_{3/2}$ and $2p_{1/2}$ suggest the presence of Ti(IV) in TiO_2 in all prepared PEO coatings regardless of the alloy or the time of the treatment [50]. The Mo $3d_{5/2}$ and Mo $3d_{3/2}$ XPS peaks at 231.8 and 235.0 eV, respectively, are ascribable to a 3d doublet of Mo(VI) in Na_2MoO_4, in agreement with XRD

data [51]. The doublet of Fe 2p (at 709.8 and 723.5 eV for $Fe2p_{3/2}$ and $2p_{1/2}$, respectively) is ascribable to Fe(III) in Fe_2O_3 [51] in agreement with XRD data. Both G2 PEO coatings show an O 1s peak, which is the sum of three contributions at 530.3, 531.3, and 532.5 eV, respectively. The one at lower BEs is characteristic of reticular oxygen of TiO_2 and Fe_2O_3, the one in the middle is ascribable to oxygen bond to Mo(VI), while the contribution of higher BEs is distinctive of oxygen in phosphates [51]. The XPS core level of P 2p also confirms the presence of this last species. The peak positions (132.5 and 133.5 eV) of two components of the doublet $P 2p_{3/2}$ and $2p_{1/2}$ well agree with P(V) in phosphates [51]. This agrees with the XRD data, which demonstrated the presence of Na_3PO_4. In the G5 PEO coatings, another contribution at 534.6 eV, which becomes more significant on the sample G5-60, is present in the O 1s region. This could be due to absorbed moisture.
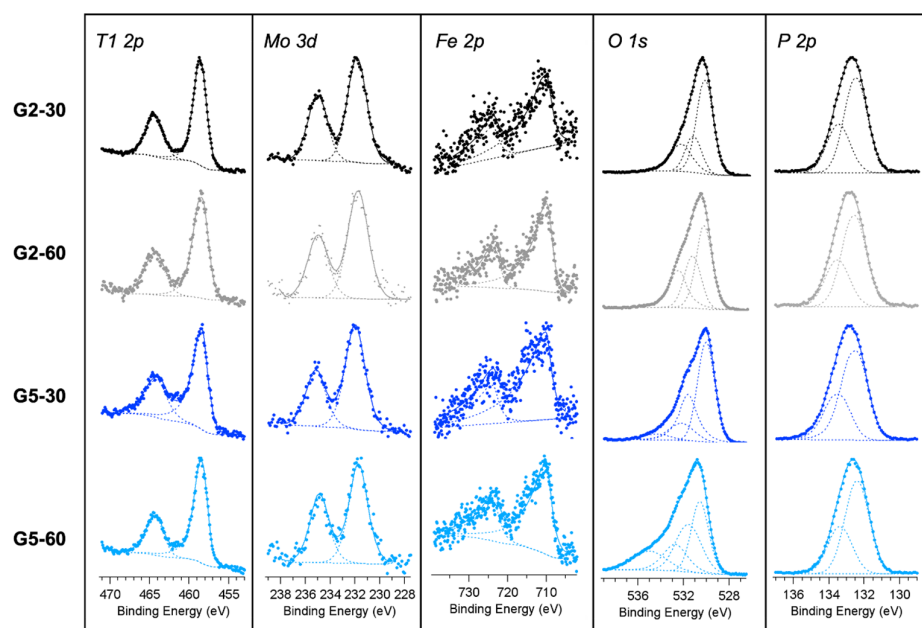
Figure 6. XPS peaks of PEO coatings formed at 30 and 60 min: XPS core levels of Ti 2p, Mo 3d, Fe 2p, P 2p, and O 1s are shown. (Black is used for the sample G2-30, gray for the sample G2-60, dark blue for the sample G5-30 and light blue for the sample G5-60).

In Table 4, the XPS atomic composition is shown. The quantitative analysis reveals a higher amount of oxygen and phosphorus, which agrees with the formation on the surface of phosphate species.

Table 4. XPS atomic percentage recorded on the different samples.

Sample	O%	P%	Ti%	Fe%	Mo%
G2-30	76.3	17.0	5.5	0.6	0.6
G2-60	78.2	16.6	4.0	0.9	0.2
G5-30	79.0	17.9	2.0	0.9	0.2
G5-60	80.1	16.3	2.2	1.3	0.2

3.4. Corrosion Resistance of Black Coatings

The corrosion resistance of PEO coatings, formed on two distinct titanium alloys, G2 and G5, through two different treatment durations (30 and 60 min), was evaluated using both PDP and EIS tests. It is important to note that PEO coatings are robust ceramic insulating coatings, which limited the utility of PDP primarily to qualitative assessments among the coatings and the original, untreated titanium alloys. Due to the inapplicability of the Tafel law [52], quantitative analysis was not possible. Figure 7 indicates the polarization

curves, showing improved corrosion resistance for samples subjected to 60 min of PEO treatment on both titanium alloys, G2 and G5. The noticeable shift towards lower current densities, spanning up to one order of magnitude, demonstrates the improved corrosion resistance of the PEO-treated samples compared to the untreated titanium alloys. This transition occurs in the following order: substrate coated for 60 min > substrate coated for 30 min > uncoated substrate. Furthermore, shifting the corrosion potential in the PEO-treated samples toward the anodic position indicates improved corrosion resistance. Such a shift towards a more positive corrosion potential typically implies greater thermodynamic stability for the tested specimens [14].
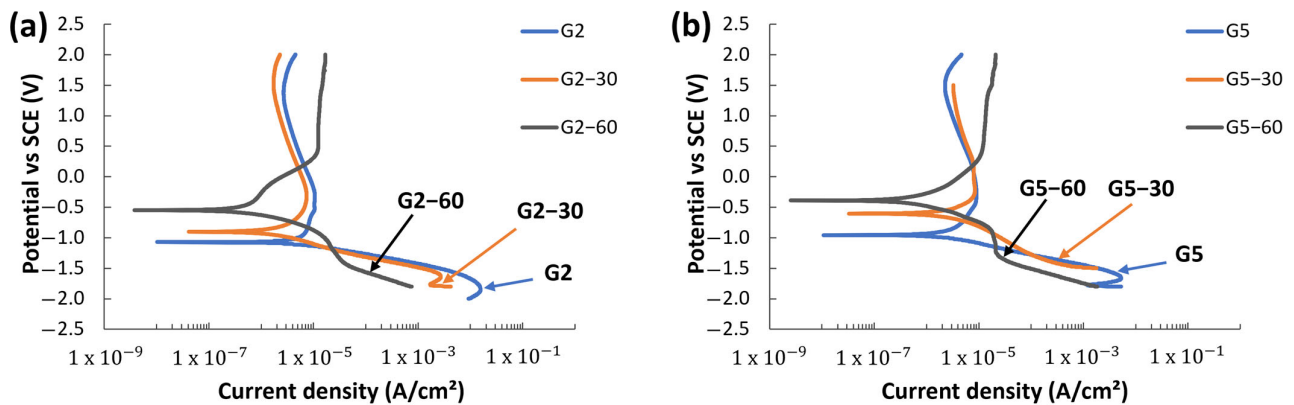

Figure 7. Potentiodynamic polarization (PDP) curves of the PEO-coated samples and as-received titanium alloys: (**a**) G2 and (**b**) G5 at the 3.5% NaCl.

EIS measurements were carried out to better understand the corrosion resistance of the PEO coatings. EIS measurements were performed under the same conditions as PDP at room temperature in 3.5% NaCl. Results from the EIS test are presented in the form of Bode plots, Figure 8, and Nyquist plots, Figure 9. As seen from both plots for G2 titanium alloy (indicated with the letter a), sample G2-60 has the highest impedance value through all applied frequencies. A higher value of the impedance indicates a better corrosion resistance of the system. From the Bode Modulus plot and the Nyquist plot for G5 titanium alloy (indicated with the letter b), sample G5-30 shows a higher impedance value at higher frequencies, while sample G5-60 shows a higher impedance value at lower frequencies. Generally speaking, the corrosion resistance of titanium alloys is improved by PEO coatings. Bode plot representation of phase angle (Zphz) as a function of frequency can be used to visualize the relative contributions of capacitive and resistive elements, with ideal capacitance at Zphz = $-90°$ and resistive processes indicated by Zphz = 0 [53]. Capacitive behavior is observed mainly at medium and low frequencies, while resistive behavior is evident at high frequencies. All four samples coated with PEO have a two-time constant compared to a one-time constant in pure titanium alloys. The first-time constant appears in the high-frequency region with a minimum of about 10^4 Hz, while the second appears in the low-frequency region with a minimum of about 10^0 Hz. It proves the presence of two layers in PEO coatings—an external porous layer and an internal barrier layer—in line with our previous research on PEO coatings [54,55] and the work of Mohedano et al. [56]. A one-time constant in the as-received samples indicates the presence of only an oxide layer.
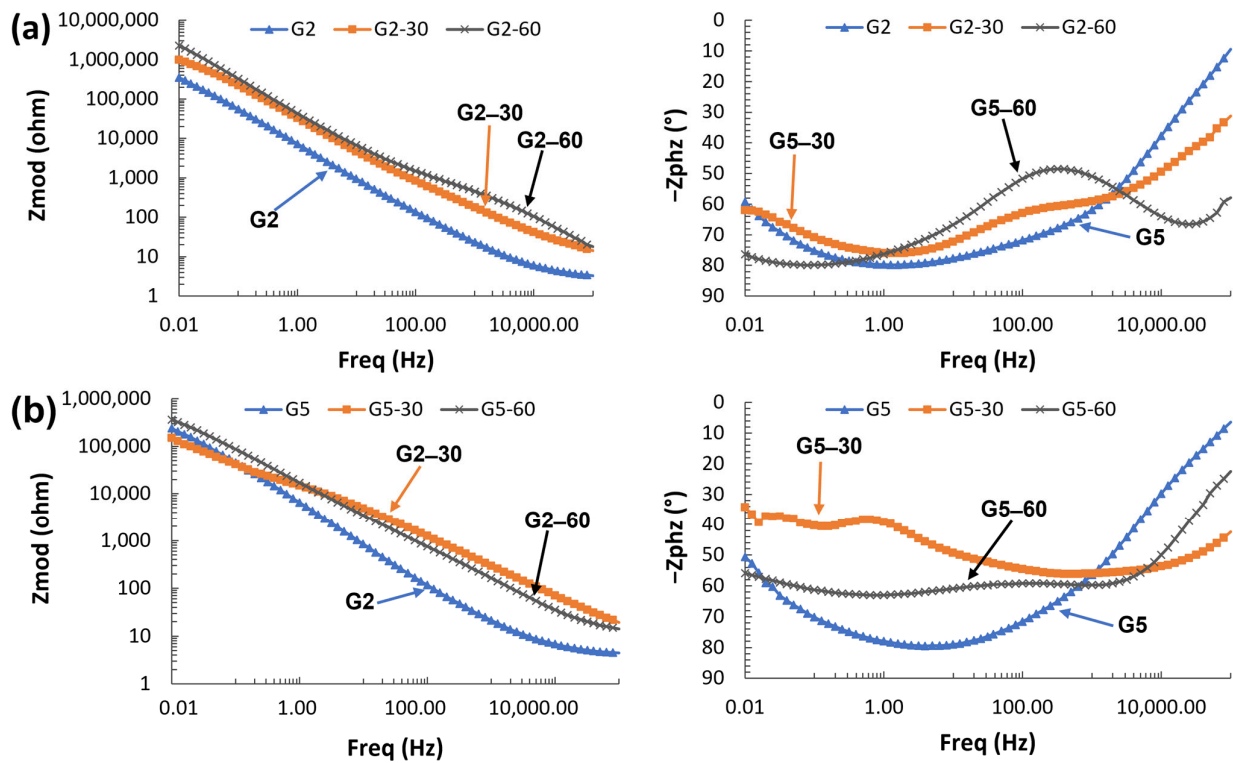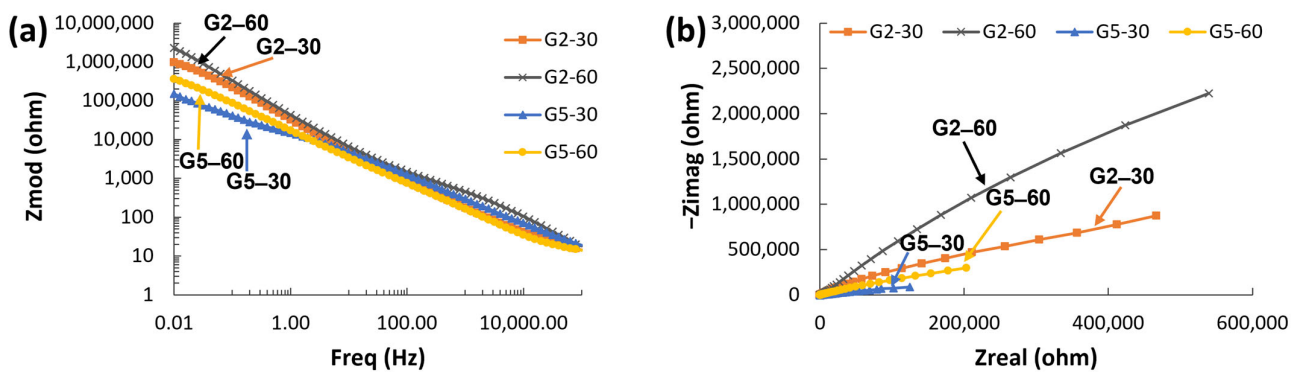
Figure 8. Results of the EIS tests in the form of Bode Modulus plots (impedance vs. frequency (Zmod vs. Freq)) and Bode Phase plots (phase vs. frequency (Zphz vs. Freq)) for the (**a**) PEO-coated samples on the G2 titanium alloy and the G2 titanium alloy without the coating; (**b**) PEO-coated samples on the G5 titanium alloy and the G5 titanium alloy without the coating.
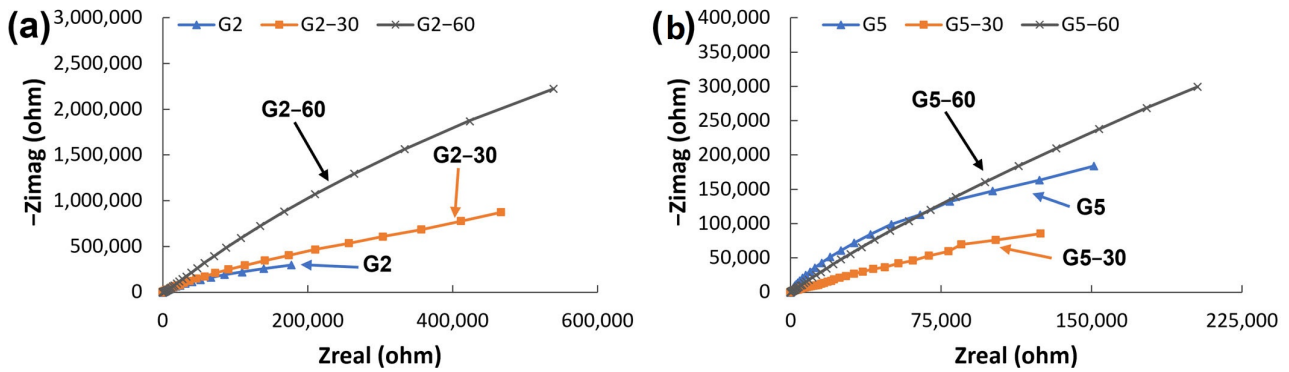
Figure 9. Results of the EIS tests in the form of Nyquist plots (impedance vs. frequency (−Zimag vs. Zreal)) for the: (**a**) PEO-coated samples on the G2 titanium alloy and the G2 titanium alloy without the coating; (**b**) PEO-coated samples on the G5 titanium alloy and the G5 titanium alloy without the coating.

To compare samples with only PEO coatings, the results, including PEO coatings on both titanium alloys, G2 and G5, are shown in the form of a Bode Modulus plot and Nyquist plot in Figure 10. In general, the corrosion resistance of PEO-coated samples on G2 titanium alloy is better than that of samples on G5 alloy, while the best corrosion resistance is found in sample G2-60. The larger arcs on the Nyquist graph and higher impedance values support this conclusion.

Figure 10. Results of the EIS tests in the form of (**a**) Bode Modulus plot (impedance vs. frequency (Zmod vs. Freq)) and (**b**) Nyquist plot (impedance vs. frequency (−Zimag vs. Zreal)) for the PEO-coated samples on the G2 titanium alloy and the G5 titanium alloy.

EIS data were fitted, applying two distinct equivalent electrical circuits for quantitative assessments of the PEO-coated samples. One circuit was designed for untreated samples (Figure 11a), while the other was developed for PEO-treated samples (Figure 11b). Since the untreated sample contained just a natural oxide layer, it was examined using a simple Randles $R_s(R_o CPE_o)$ circuit configuration. On the other hand, the analysis of PEO-treated samples required a dual-circuit $R_s(R_p CPE_p(R_b CPE_b))$ configuration due to the presence of two distinct layers: an external porous layer and an internal barrier layer. A Constant Phase Element (*CPE*) was used in both electrical circuits, according to the typically less-than-ideal nature of capacitance measurements [57]. *CPE* can be represented as follows:

$$Z = (1/Y_0)/(j\omega)^\alpha \tag{2}$$
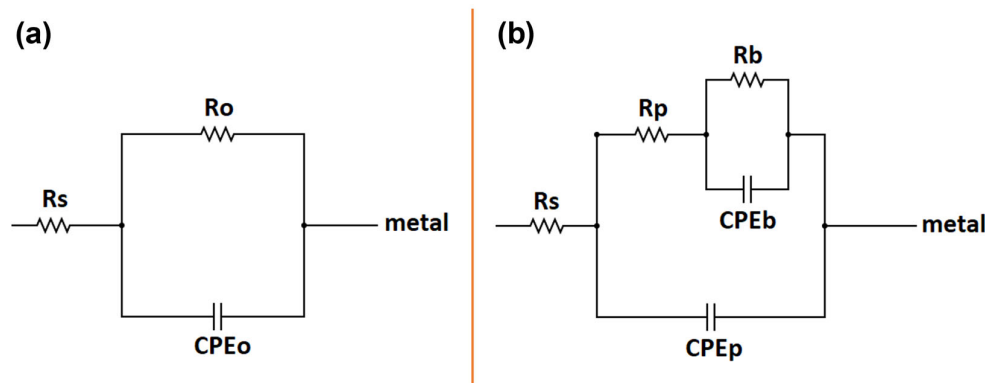
Figure 11. Equivalent electrical circuits employed to fit the EIS data, (**a**) simple Randles circuit $R_s(R_o CPE_o)$; (**b**) dual-circuit $R_s(R_p CPE_p(R_b CPE_b))$.

In the given expression, Y_0 represents a constant phase element (*CPE*), ω stands for angular frequency, and α is an empirical exponent. α can assume a value of 1, indicating a perfect capacitor, and 0 perfect resistor. Within the equivalent circuit, various components are delineated: R_s, which signifies the resistance of the solution; R_o, serving as a measure of the corrosion resistance of the natural oxide layer; R_p, indicative of the corrosion resistance of the porous layer; and R_b, representing the corrosion resistance of the barrier layer. A *CPE* includes (CPE_o) connected to the oxide layer, (CPE_p) connected to the porous layer, and (CPE_b) connected to the barrier layer.

The fitting results of the experimental EIS data are reported in Table 5 in the case of the PEO-coated samples and Table 6 for the as-received samples. Good fitting results were obtained, as confirmed by chi-squared values varying around 0.01 and 0.001.

Table 5. Results of the experimental EIS data fitting with the equivalent electrical circuit for the PEO-coated samples.

	G2-30	G2-60	G5-30	G5-60
Rs $[\Omega \, cm^2]$	11.59	3.90	5.40	9.67
Rp $[\Omega \, cm^2]$	36.07×10^4	13.07×10^2	28.82×10^3	22.72×10^5
Rb $[\Omega \, cm^2]$	26.47×10^5	17.12×10^7	22.68×10^4	51.19×10^4
$Yo_p \, [S \, s^\alpha cm^{-2}]$	10.00×10^{-6}	16.09×10^{-7}	13.20×10^{-6}	15.70×10^{-6}
α_p	0.73	0.79	0.63	0.69
$Yo_b \, [S \, s^\alpha cm^{-2}]$	80.62×10^{-7}	30.12×10^{-7}	26.50×10^{-6}	44.05×10^{-6}
α_b	0.86	0.86	0.72	0.87
χ^2	82.99×10^{-3}	56.82×10^{-4}	12.00×10^{-4}	18.67×10^{-4}

Table 6. Results of the experimental EIS data fitting with the equivalent electrical circuit for the as-received samples.

	G2	G5
Rs $[\Omega \, cm^2]$	3.61	4.89
Ro $[\Omega \, cm^2]$	13.30×10^5	50.83×10^4
$Yo_o \, [S \, s^\alpha cm^{-2}]$	28.71×10^{-6}	33.71×10^{-6}
α_o	0.85	0.84
χ^2	11.59×10^{-3}	10.10×10^{-3}

A two order of magnitude increase in the corrosion resistance (considering both Rp and Rb) was observed for the 60-minute treated samples on the G2 titanium alloy (G2-60) compared to the 30-minute treated sample (G2-30). Furthermore, a similar value of the Yob for the G2-60 and G2-30 indicated that prolonged processing time had no significant effect on coating growth. These results showed a considerable increase in the corrosion resistance value due to the improved compactness of the coating and a thicker barrier layer, confirmed by SEM images.

Compared to PEO coatings on G2 titanium alloy, the corrosion resistance values (regarding both Rp and Rb) of PEO coatings on G5 are lower even by three orders of magnitude, which is compatible with potentiodynamic results. G5-60 shows higher values in corrosion resistance compared to sample G5-30. Similarly, the values of Yob do not change significantly, so we can conclude that the increase in corrosion resistance did not result from an increase in coating size but an increase in coating compactness. Overall, a PEO coating on both titanium alloys appears to increase corrosion resistance compared to uncoated samples, except for sample G5-30, which showed a slight decrease.

4. Discussion

According to the optical analysis, all PEO-coated samples have an absorptance greater than 0.80, indicating a black appearance. Similar outcomes can be found in the existing literature [13], where black coatings are typically reported to have solar absorptance values ranging from 0.75 to 0.90. Yao et al. [39] stated that the resulting coatings with an average solar absorbance value of 0.76 were deemed appropriate for application in optical components aboard spacecraft. Notably, the coatings have significant differences, especially when examining the same titanium alloy but subjected to a longer PEO process duration. The coating's absorptance increases as the process time is extended. Coatings produced during the 60-minute PEO process absorb up to 86% of radiation, and this difference is visible in stereo microscope images. A more expressive black color is confirmed compared to 30-minute PEO coatings.

The blackness of the coatings is affected by anions such as VO^{3-}, WO_4^{2-}, MoO_4^{2-} and transition metal cations such as Fe^{2+}, Fe^{3+}, Cu^{2+}, Co^{2+}, Ni^{2+} and Zr^{4+}, according to the literature [19,26,34]. Regarding our present study, additives based on molybdenum and iron were used. XRD analysis showed that Fe^{3+} and MoO_4^{2-} were successfully incorporated

into all prepared coatings. XPS and EDS analysis further confirmed the presence of these species.

As well as cations and anions, the black color of the coatings is influenced by the microstructure. Irregular surfaces and micro-pores of the coatings constitute optical traps, increasing multiple reflections of incident light on the surface of the coatings and resulting in a decrease in the reflectivity [9,41]. Micro-pores dimensions correspond to the infrared spectral range. The surface SEM examination reveals the formation of a channel-like structure, which arises from the interconnection of nano-pores after 30 min. This particular microstructure might be one of the contributing factors to the increased absorptance in samples subjected to extended PEO treatment times. The nano-pores, on the other hand, are most likely too small to accommodate light waves.

Additionally, Han et al. [14] reported that the black color comes from the titanium ions themselves incorporated into the titanium dioxide. They believe that Ti^{3+} and Ti^{2+} from the Ti-6Al-4V substrate are responsible for the black color of TiO_2. Nevertheless, it is known that TiO_2 is mainly used as a white pigment [58–60].

All PEO-coated samples have better corrosion resistance than bare titanium alloys, G2 and G5, as confirmed by PDP measurements. Based on PDP analysis, the literature [14,37,38] also reported improved corrosion performance when using black PEO coatings on titanium alloys in 3.5 wt.% NaCl solution. Despite the PDP curves shifting towards lower current densities and more positive potentials, a higher anodic current is evident in the case of 60-minute samples for both titanium alloys, G2 and G5 (Figure 7). A similar occurrence was noted by Han et al. [14], who ascribed this phenomenon to the increased formation of rutile due to repeated PEO discharges in the coatings formed at longer treatment times, and Madhuri et al. [37] noted that the presence of rutile contributes to better corrosion resistance, particularly when exposed to a NaCl solution [49].

Furthermore, upon examining the results of the EIS tests, the distinctions between the samples are apparent. Those produced after a 60-minute PEO process display improved corrosion resistance. This heightened resistance can be attributed to a thicker inner barrier layer and, in general, more compact coatings, as demonstrated by SEM cross-section observations. Compactness, uniformity, and interfacial stability are recognized as crucial factors that dictate the protective effectiveness of oxide coatings. The presence of porosity and inadequate interfacial adhesion between the coatings and the substrate can facilitate the infiltration of corrosive agents into the coating, leading to substrate damage and, consequently, rapid surface pitting [28]. Similar results were found in the literature, where it was reported that the better corrosion resistance for the thin coatings was attributed to the denser, more homogeneous inner (barrier) layer [14,61]. In addition to SEM observation, the presence of two distinct layers in PEO coatings is also discernible from the appearance of two-time constants on the Bode Phase plots (Figure 8) of PEO-coated titanium alloys. The time constant observed at high frequencies corresponds to the porous (outer) layer, while the second time constant is associated with the inner (barrier) layer. In contrast, untreated samples exhibit only a single time constant. These findings align with previously published research on PEO coatings applied to titanium substrates [28,62].

The enhancement of the barrier layer is particularly evident in the samples of the G2 titanium alloy. Based on the fitting values of the EIS measurements, sample G2-60 shows even two orders of magnitude higher corrosion resistance in the barrier layer compared to G2-30 (Table 5). Overall, G2 coatings exhibit superior corrosion resistance compared to G5 coatings, and the G2 coating prepared after the prolonged PEO process time of 60 min stands out as the best with the corrosion resistance of $17.12 \times 10^7 \, \Omega \, cm^2$. This can be related to the improved corrosion resistance of the substrate (G2 titanium behaves better than G5 titanium), with an oxide layer resistance of $13.30 \times 10^5 \, \Omega \, cm^2$ and $50.83 \times 10^4 \, \Omega \, cm^2$, respectively. These values are consistent with the corrosion resistance exhibited by similar PEO coatings on titanium alloys. For instance, Molaei et al. [62] reported silicate-based PEO coatings on the G2 titanium alloy with resistance values in the $10^6 \, \Omega \, cm^2$ range, while Fattah-Alhosseini et al. [63] observed phosphate-based

PEO coatings with resistance values in the 10^5 Ω cm^2 range. When focusing solely on titanium substrates within the existing literature, it is again evident that G2 titanium alloy exhibits greater corrosion resistance [62] than G5 titanium alloy [64]. Various PEO process parameters, including electrolyte concentration, composition, processing time, and current density, influence the corrosion resistance of PEO coatings [37]. These factors lead to variations in the coating's chemical composition, thickness, and compactness, ultimately affecting its corrosion resistance [49]. Due to these variables, it is only feasible to provide a broad comparison of coatings found in different literature sources.

5. Conclusions

Effective black ceramic coatings were successfully obtained on G2 and G5 titanium alloy with the PEO process. The coatings were prepared to work in direct-current mode at a constantly low current density of 0.05 A/cm^2. The difference between coatings generated at 30 min and 60 min was investigated. A novel combination of additives (FeSO$_4$ and (NH$_4$)$_6$Mo$_7$O$_{24}$), not previously documented in the literature, was employed as coloring agents. The following conclusions can be drawn after examining the optical, morphological, structural, chemical, and electrochemical characterization.

(A) All the coatings generated possess a near 10% reflectance in the visible spectrum and a peak reflectance of around 35% in the NIR range. Under all tested conditions, the calculated absorptance of the coatings exceeds 0.8, reaching a maximum peak of 0.86 in the instance of PEO coatings prepared following a 60-minute duration.

(B) The surface SEM images clearly demonstrate that the nano-pores are stacked and connected after 60 min of the PEO process, forming micro-pores and a particular channel structure. Since this morphology is suitable for trapping light waves, the coatings provide a deeper black color. Cross-sectional SEM micrographs show no difference in coating size after the PEO process is extended, but there is a difference in homogeneity. After 60 min, more uniform coatings were obtained with a thicker barrier layer.

(C) According to EDS analysis of the surface and cross-section, coatings are rich in oxygen and phosphorus, with modest amounts of iron, molybdenum, and sodium. The presence of TiO$_2$ in two different mineral forms, anatase, and rutile, Na$_3$PO$_4$, γFe$_2$O$_3$ and Na$_2$MoO$_4$, is confirmed by XRD and XPS.

(D) From the PDP, the noticeable shift of the current density towards lower current densities demonstrates the improved corrosion resistance of the PEO-treated samples compared to the untreated titanium alloys. The improvement is noticeable in G2 and G5 titanium alloy and at both PEO process times.

(E) The EIS confirms that the coatings on G2 titanium are more corrosion-resistant than G5. The internal barrier layer of G2 titanium, in particular, exhibits significantly higher resistance, and G2-60 stands out as the best coating in terms of corrosion resistance, with an internal barrier resistance of 17.12 $\times$ 10^7 Ω.

Author Contributions: Conceptualization, L.P. and M.D.; methodology, L.P. and K.B.; software, L.K. and M.M.N.; validation, L.K.; formal analysis, L.K., M.M.N. and E.C.; investigation, L.K., M.M.N., E.C. and L.P.; resources, K.B., M.D. and M.M.N.; data curation, L.K., M.M.N., E.C. and L.P.; writing—original draft preparation, L.K.; writing—review and editing, L.P., M.M.N. and E.C.; visualization, L.K.; supervision, K.B., M.D. and L.P.; project administration, K.B. and M.D.; funding acquisition, K.B. and M.D. All authors have read and agreed to the published version of the manuscript.

Institutional Review Board Statement: Not applicable.

Informed Consent Statement: Not applicable.

Conflicts of Interest: The authors declare no conflict of interest.

References

1. Uma Rani, R.; Sharma, A.K.; Minu, C.; Poornima, G.; Tejaswi, S. Studies on Black Electroless Nickel Coatings on Titanium Alloys for Spacecraft Thermal Control Applications. *J. Appl. Electrochem.* **2010**, *40*, 333–339. [CrossRef]
2. Han, G.; Zhang, Y. Microstructure and Corrosion of Laser Cladding Coatings on Titanium Alloy with Nd_2O_3. *J. Eng. Mater. Technol. Trans. ASME* **2021**, *143*, 011007. [CrossRef]
3. Ramazanova, Z.M.; Zamalitdinova, M.G. Study of the Properties of Qxide Coatings Formed on Titanium by Plasma Electrolytic Oxidation Method. *Eurasian Chem. Technol. J.* **2020**, *22*, 51–58. [CrossRef]
4. Li, G.J.; Li, J.; Luo, X. Effects of High Temperature Treatment on Microstructure and Mechanical Properties of Laser-Clad NiCrBSi/WC Coatings on Titanium Alloy Substrate. *Mater. Charact.* **2014**, *98*, 83–92. [CrossRef]
5. Guo, Q.; Xu, D.; Yang, W.; Guo, Y.; Yang, Z.; Li, J.; Gao, P. Synthesis, Corrosion, and Wear Resistance of a Black Microarc Oxidation Coating on Pure Titanium. *Surf. Coat. Technol.* **2020**, *386*, 125454. [CrossRef]
6. Yılmaz, E.; Çakıroğlu, B.; Gökçe, A.; Findik, F.; Gulsoy, H.O.; Gulsoy, N.; Mutlu, Ö.; Özacar, M. Novel Hydroxyapatite/Graphene Oxide/Collagen Bioactive Composite Coating on Ti16Nb Alloys by Electrodeposition. *Mater. Sci. Eng. C* **2019**, *101*, 292–305. [CrossRef]
7. Gupta, P.; Fang, F.; Rubanov, S.; Loho, T.; Koo, A.; Swift, N.; Fiedler, H.; Leveneur, J.; Murmu, P.P.; Markwitz, A.; et al. Decorative Black Coatings on Titanium Surfaces Based on Hard Bi-Layered Carbon Coatings Synthesized by Carbon Implantation. *Surf. Coat. Technol.* **2019**, *358*, 386–393. [CrossRef]
8. Köse, R.; Urtekin, L.; Ceylan, A.; Salman, S.; Findik, F. Three Types of Ceramic Coating Applicability in Automotive Industry for Wear Resistance Purpose. *Ind. Lubr. Tribol.* **2005**, *57*, 140–144. [CrossRef]
9. Yao, R.; Li, Y.; Yao, Z.; Zhang, P.; Lu, S.; Wu, X. Black PEO Coating with Enhanced Thermal Stability on Titanium Alloy and Its Thermal Control Properties. *Surf. Coat. Technol.* **2022**, *429*, 127934. [CrossRef]
10. Tu, W.; Zhu, Z.; Zhuang, X.; Cheng, Y.; Skeldon, P. Effect of Frequency on Black Coating Formation on AZ31 Magnesium Alloy by Plasma Electrolytic Oxidation in Aluminate-Tungstate Electrolyte. *Surf. Coat. Technol.* **2019**, *372*, 34–44. [CrossRef]
11. Tu, W.; Cheng, Y.; Wang, X.; Zhan, T.; Han, J.; Cheng, Y. Plasma Electrolytic Oxidation of AZ31 Magnesium Alloy in Aluminate-Tungstate Electrolytes and the Coating Formation Mechanism. *J. Alloys Compd.* **2017**, *725*, 199–216. [CrossRef]
12. Goueffon, Y.; Arurault, L.; Mabru, C.; Tonon, C.; Guigue, P. Black Anodic Coatings for Space Applications: Study of the Process Parameters, Characteristics and Mechanical Properties. *J. Mater. Process. Techno.l* **2009**, *209*, 5145–5151. [CrossRef]
13. Arunnellaiappan, T.; Rama Krishna, L.; Anoop, S.; Uma Rani, R.; Rameshbabu, N. Fabrication of Multifunctional Black PEO Coatings on AA7075 for Spacecraft Applications. *Surf. Coat. Technol.* **2016**, *307*, 735–746. [CrossRef]
14. Han, J.; Cheng, Y.; Tu, W.; Zhan, T.Y.; Cheng, Y. The Black and White Coatings on Ti-6Al-4V Alloy or Pure Titanium by Plasma Electrolytic Oxidation in Concentrated Silicate Electrolyte. *Appl. Surf. Sci.* **2018**, *428*, 684–697. [CrossRef]
15. Rakoch, A.G.; Van Tuan, T.; Khabibullina, Z.V.; Blawert, C.; Serdechnova, M.; Scharnagl, N.; Zheludkevich, M.L.; Gladkova, A.K.A. Role of Cobalt Additive on Formation and Anticorrosion Properties of PEO Coatings on AA2024 Alloy in Alkali-Silicate Electrolyte. *Surf. Coat. Technol.* **2022**, *433*, 128075. [CrossRef]
16. Salman, S.; Köse, R.; Urtekin, L.; Findik, F. An Investigation of Different Ceramic Coating Thermal Properties. *Mater. Des.* **2006**, *27*, 585–590. [CrossRef]
17. Takadoum, J. Black Coatings: A Review. *EPJ Appl. Phys.* **2010**, *52*, 559–564. [CrossRef]
18. Dou, Q.; Li, W.; Zhang, G.; Wan, X. Preparation and Characterisation of Black Ceramic Coating on AZ91D Magnesium Alloy by Plasma Electrolytic Oxidation with Reduced Energy Consumption. *Mater. Res. Innov.* **2015**, *19*, S223–S227. [CrossRef]
19. Pillai, A.M.; Rajendra, A.; Sharma, A.K.; Bera, P.; Poornima, S.; Sampath, S. Development of Vanadium Impregnated Flat Absorber Composite PEO Coating on AA6061 Alloy. *Surf. Coat. Technol.* **2021**, *410*, 126891. [CrossRef]
20. Wang, Y.; Jiang, Z.; Yao, Z. Effects of Na2WO$_4$ and Na_2SiO_3 Additives in Electrolytes on Microstructure and Properties of PEO Coatings on Q235 Carbon Steel. *J. Alloys Compd.* **2009**, *481*, 725–729. [CrossRef]
21. Li, H.; Lu, S.; Wu, X.; Qin, W. Influence of Zr^{4+} Ions on Solar Absorbance and Emissivity of Coatings Formed on AZ31 Mg Alloy by Plasma Electrolytic Oxidation. *Surf. Coat. Technol.* **2015**, *269*, 220–227. [CrossRef]
22. Yi, A.; Liao, Z.; Zhu, W.; Zhu, Z.; Li, W.; Li, K.; Chen, K.; Huang, S. Influence of Electrolyte Temperature on the Color Values of Black Plasma Electrolytic Oxidation Coatings on AZ31B Mg Alloy. *Coatings* **2020**, *10*, 890. [CrossRef]
23. Shrestha, S.; Shashkov, P. Dunn, Microstructural and thermo-optical properties of black keronite peo coating on aluminium alloy aa7075 for spacecraft materials applications. In Proceedings of the 10th ISMSE & the 8th ICPMSE, Collioure, France, 19–23 June 2006.

24. Sikdar, S.; Menezes, P.V.; Maccione, R.; Jacob, T.; Menezes, P.L. Plasma Electrolytic Oxidation (Peo) Process—Processing, Properties, and Applications. *Nanomaterials* **2021**, *11*, 1375. [CrossRef]

25. Wang, L.; Zhou, J.; Liang, J.; Chen, J. Thermal Control Coatings on Magnesium Alloys Prepared by Plasma Electrolytic Oxidation. *Appl. Surf. Sci.* **2013**, *280*, 151–155. [CrossRef]

26. Pan, J.; Wen, Y.; Wang, L.; Wu, Z.; Dong, H.; Ye, Z. Doping and Defects: The Coloring Mechanism of Black Plasma Electrolytic Oxidation (PEO) Films on Aluminum Alloys. *Surf. Coat. Technol.* **2022**, *431*, 128035. [CrossRef]

27. Akbari, E.; Di Franco, F.; Ceraolo, P.; Raeissi, K.; Santamaria, M.; Hakimizad, A. Electrochemically-Induced TiO2 Incorporation for Enhancing Corrosion and Tribocorrosion Resistance of PEO Coating on 7075 Al Alloy. *Corros. Sci.* **2018**, *143*, 314–328. [CrossRef]

28. Nagumothu, R.B.; Thangavelu, A.; Nair, A.M.; Sukumaran, A.; Anjilivelil, T. Development of Black Corrosion-Resistant Ceramic Oxide Coatings on AA7075 by Plasma Electrolytic Oxidation. *Trans. Indian Inst. Met.* **2019**, *72*, 47–53. [CrossRef]

29. Rakoch, A.G.; Kuznetsov, Y.I.; van Tuan, T.; Khabibullina, Z.V.; Gladkova, A.A.; Chirkunov, A.A.; Semiletov, A.M. Black Decorative Anticorrosion Coatings Obtained on Aa2024 Alloy by Plasma–Electrolytic Treatment and Inhibition. *Int. J. Corros. Scale Inhib.* **2021**, *10*, 562–579. [CrossRef]

30. Zhu, M.; Song, Y.; Liu, Z.; Xu, D.; Dong, K.; Han, E.H. Optimization of Thermal Control and Corrosion Resistance of PEO Coatings on 7075 Aluminum Alloy by Frequency Alteration. *Surf. Coat. Technol.* **2022**, *446*, 128797. [CrossRef]

31. Aliramezani, R.; Raeissi, K.; Santamaria, M.; Hakimizad, A. Characterization and Properties of PEO Coatings on 7075 Al Alloy Grown in Alkaline Silicate Electrolyte Containing $KMnO_4$ Additive. *Surf. Coat. Technol.* **2017**, *329*, 250–261. [CrossRef]

32. Hwang, I.J.; Shin, K.R.; Lee, J.S.; Ko, Y.G.; Shin, D.H. Formation of Black Ceramic Layer on Aluminum Alloy by Plasma Electrolytic Oxidation in Electrolyte Containing Na_2WO_4. *Mater. Trans.* **2012**, *53*, 559–564. [CrossRef]

33. Tang, H.; Sun, Q.; Yi, C.G.; Jiang, Z.H.; Wang, F.P. High Emissivity Coatings on Titanium Alloy Prepared by Micro-Arc Oxidation for High Temperature Application. *J. Mater. Sci.* **2012**, *47*, 2162–2168. [CrossRef]

34. Yao, Z.; Li, X.; Wei, H.; Xia, Q.; Wang, Y.; Li, D.; Jiang, Z. Black Ceramic Coatings on Ti Alloy with Enhanced High Absorptivity and High Emissivity by Plasma Electrolytic Oxidation. *Int. J. Appl. Ceram. Technol.* **2019**, *16*, 994–1003. [CrossRef]

35. Tang, H.; Xin, T.; Sun, Q.; Yi, C.; Jiang, Z.; Wang, F. Influence of $FeSO_4$ Concentration on Thermal Emissivity of Coatings Formed on Titanium Alloy by Micro-Arc Oxidation. *Appl. Surf. Sci.* **2011**, *257*, 10839–10844. [CrossRef]

36. Tang, H.; Sun, Q.; Xin, T.; Yi, C.; Jiang, Z.; Wang, F. Influence of $Co(CH_3COO)_2$ Concentration on Thermal Emissivity of Coatings Formed on Titanium Alloy by Micro-Arc Oxidation. *Curr. Appl. Phys.* **2012**, *12*, 284–290. [CrossRef]

37. Madhuri, D.; Ghosh, R.; Hasan, M.A.; Dey, A.; Pillai, A.M.; Anantharaju, K.S.; Rajendra, A. Development and Characterization of High Emittance and Low-Thickness Plasma Electrolytic Oxidation Coating on Ti6Al4V for Spacecraft Application. *J. Mater. Eng. Perform.* **2021**, *30*, 4072–4082. [CrossRef]

38. Madhuri, D.; Ghosh, R.; Hasan, M.A.; Dey, A.; Pillai, A.M.; Angamuthu, M.; Anantharaju, K.S.; Rajendra, A. Flat Absorber Black PEO Coatings on Ti6Al4V for Spacecraft Thermal Control Application. *Ceram. Int.* **2022**, *48*, 35906–35914. [CrossRef]

39. Yao, Z.; Hu, B.; Shen, Q.; Niu, A.; Jiang, Z.; Su, P.; Ju, P. Preparation of Black High Absorbance and High Emissivity Thermal Control Coating on Ti Alloy by Plasma Electrolytic Oxidation. *Surf. Coat. Technol.* **2014**, *253*, 166–170. [CrossRef]

40. Yao, Z.; Shen, Q.; Niu, A.; Hu, B.; Jiang, Z. Preparation of High Emissivity and Low Absorbance Thermal Control Coatings on Ti Alloys by Plasma Electrolytic Oxidation. *Surf. Coat. Technol.* **2014**, *242*, 146–151. [CrossRef]

41. Yao, Z.; Xia, Q.; Shen, Q.; Ju, P.; Su, P.; Hu, B.; Jiang, Z. A Facile Preparation of Ceramic Coatings on Ti Alloys for Thermal Protection Systems. *Sol. Energy Mater. Sol. Cells* **2015**, *143*, 236–241. [CrossRef]

42. Yao, Z.; Su, P.; Shen, Q.; Ju, P.; Wu, C.; Zhai, Y.; Jiang, Z. Preparation of Thermal Control Coatings on Ti Alloy by Plasma Electrolytic Oxidation in K2ZrF6 Solution. *Surf. Coat. Technol.* **2015**, *269*, 273–278. [CrossRef]

43. Miura, H.; Kobayashi, M.; Aoba, T.; Aoyama, H.; Benjanarasuth, T. An Approach for Room-Temperature Multi-Directional Forging of Pure Titanium for Strengthening. *Mater. Sci. Eng. A* **2018**, *731*, 603–608. [CrossRef]

44. Katumba, G.; Olumekor, L.; Forbes, A.; Makiwa, G.; Mwakikunga, B.; Lu, J.; Wäckelgård, E. Optical, Thermal and Structural Characteristics of Carbon Nanoparticles Embedded in ZnO and NiO as Selective Solar Absorbers. *Sol. Energy Mater. Sol. Cells* **2008**, *92*, 1285–1292. [CrossRef]

45. Schneider, C.A.; Rasband, W.S.; Eliceiri, K.W. NIH Image to ImageJ: 25 Years of Image Analysis. *Nat. Methods* **2012**, *9*, 671–675. [CrossRef]

46. Mazinani, A.; Nine, M.J.; Chiesa, R.; Candiani, G.; Tarsini, P.; Tung, T.T.; Losic, D. Graphene Oxide (GO) Decorated on Multi-Structured Porous Titania Fabricated by Plasma Electrolytic Oxidation (PEO) for Enhanced Antibacterial Performance. *Mater. Des.* **2021**, *200*, 109443. [CrossRef]

47. Malayoglu, U.; Tekin, K.C.; Shrestha, S. Influence of Post-Treatment on the Corrosion Resistance of PEO Coated AM50B and AM60B Mg Alloys. *Surf. Coat. Technol.* **2010**, *205*, 1793–1798. [CrossRef]

48. Gaurav, G.; Sharma, A.; Dangayach, G.S.; Meena, M.L. Assessment of Jojoba as a Pure and Nano-Fluid Base Oil in Minimum Quantity Lubrication (MQL) Hard-Turning of Ti–6Al–4V: A Step towards Sustainable Machining. *J. Clean. Prod.* **2020**, *272*, 122553. [CrossRef]

49. Aliofkhazraei, M.; Macdonald, D.D.; Matykina, E.; Parfenov, E.V.; Egorkin, V.S.; Curran, J.A.; Troughton, S.C.; Sinebryukhov, S.L.; Gnedenkov, S.V.; Lampke, T.; et al. Review of Plasma Electrolytic Oxidation of Titanium Substrates: Mechanism, Properties, Applications and Limitations. *Appl. Surf. Sci. Adv.* **2021**, *5*, 100121. [CrossRef]

50. Galstyan, V.; Ponzoni, A.; Kholmanov, I.; Natile, M.M.; Comini, E.; Sberveglieri, G. Highly Sensitive and Selective Detection of Dimethylamine through Nb-Doping of TiO2 Nanotubes for Potential Use in Seafood Quality Control. *Sens. Actuators B Chem.* **2020**, *303*, 127217. [CrossRef]

51. IST X-Ray PhotoElectron Spectroscopy Database, NIST Standard Reference Database 20, Version 4.1, Web Version. Available online: https://searchworks.stanford.edu/view/9742414 (accessed on 12 June 2023).

52. Pezzato, L.; Dabalà, M.; Gross, S.; Brunelli, K. Effect of Microstructure and Porosity of AlSi$_{10}$Mg Alloy Produced by Selective Laser Melting on the Corrosion Properties of Plasma Electrolytic Oxidation Coatings. *Surf. Coat. Technol.* **2020**, *404*, 126477. [CrossRef]

53. Ko, J.S.; Sassin, M.B.; Rolison, D.R.; Long, J.W. Deconvolving Double-Layer, Pseudocapacitance, and Battery-like Charge-Storage Mechanisms in Nanoscale LiMn$_2$O$_4$ at 3D Carbon Architectures. *Electrochim. Acta* **2018**, *275*, 225–235. [CrossRef]

54. Pezzato, L.; Gennari, C.; Franceschi, M.; Brunelli, K. Influence of Silicon Morphology on Direct Current Plasma Electrolytic Oxidation Process in AlSi10Mg Alloy Produced with Laser Powder Bed Fusion. *Sci. Rep.* **2022**, *12*, 14329. [CrossRef]

55. Pezzato, L.; Vranescu, D.; Sinico, M.; Gennari, C.; Settimi, A.G.; Pranovi, P.; Brunelli, K.; Dabalà, M. Tribocorrosion Properties of PEO Coatings Produced on AZ91 Magnesium Alloy with Silicate- or Phosphate-Based Electrolytes. *Coatings* **2018**, *8*, 202. [CrossRef]

56. Serdechnova, M.; Mohedano, M.; Kuznetsov, B.; Mendis, C.L.; Starykevich, M.; Karpushenkov, S.; Tedim, J.; Ferreira, M.G.S.; Blawert, C.; Zheludkevich, M.L. PEO Coatings with Active Protection Based on In-Situ Formed LDH-Nanocontainers. *J. Electrochem. Soc.* **2017**, *164*, C36–C45. [CrossRef]

57. Kostelac, L.; Pezzato, L.; Settimi, A.G.; Franceschi, M.; Gennari, C.; Brunelli, K.; Rampazzo, C.; Dabalà, M. Investigation of Hydroxyapatite (HAP) Containing Coating on Grade 2 Titanium Alloy Prepared by Plasma Electrolytic Oxidation (PEO) at Low Voltage. *Surf. Interfaces* **2022**, *30*, 101888. [CrossRef]

58. Vieira, F.T.G.; Melo, D.S.; de Lima, S.J.G.; Longo, E.; Paskocimas, C.A.; Júnior, W.S.; de Souza, A.G.; dos Santos, I.M.G. The Influence of Temperature on the Color of TiO$_2$:Cr Pigments. *Mater. Res. Bull.* **2009**, *44*, 1086–1092. [CrossRef]

59. Razali, M.N.; Alkaf, A.A.; Zuhan, M.K.N.B.M. Formulation of Water-Based White Colour Paint from Waste Titanium Dioxide. *Mater. Today Proc.* **2021**, *48*, 1905–1909. [CrossRef]

60. Haider, A.J.; Jameel, Z.N.; Al-Hussaini, I.H.M. Review on: Titanium Dioxide Applications. *Energy Procedia* **2019**, *157*, 17–29. [CrossRef]

61. Cheng, Y.; Wu, X.Q.; Xue, Z.; Matykina, E.; Skeldon, P.; Thompson, G.E. Microstructure, Corrosion and Wear Performance of Plasma Electrolytic Oxidation Coatings Formed on Ti-6Al-4V Alloy in Silicate-Hexametaphosphate Electrolyte. *Surf. Coat. Technol.* **2013**, *217*, 129–139. [CrossRef]

62. Molaei, M.; Fattah-Alhosseini, A.; Keshavarz, M.K. Influence of Different Sodium-Based Additives on Corrosion Resistance of PEO Coatings on Pure Ti. *J. Asian Ceram. Soc.* **2019**, *7*, 247–255. [CrossRef]

63. Fattah-Alhosseini, A.; Keshavarz, M.K.; Molaei, M.; Gashti, S.O. Plasma Electrolytic Oxidation (PEO) Process on Commercially Pure Ti Surface: Effects of Electrolyte on the Microstructure and Corrosion Behavior of Coatings. *Met. Mater Trans. A Phys. Met. Mater. Sci.* **2018**, *49*, 4966–4979. [CrossRef]

64. Yang, X.; Dong, X.; Li, W.; Feng, W.; Xu, Y. Effect of Solution and Aging Treatments on Corrosion Performance of Laser Solid Formed Ti-6Al-4V Alloy in a 3.5 Wt. % NaCl Solution. *J. Mater. Res. Technol.* **2020**, *9*, 1559–1568. [CrossRef]